Available online at www.sciencedirect.com
SCIENCE DIRECT®
Thermochimica Acta 426 (2005) 7–14
thermochimica acta
www.elsevier.com/locate/tca

Synthesis and properties of Nasicon-type materials

A. Ignaszak*, P. Pasierb, R. Gajerski, S. Komornicki

Faculty of Materials Science and Ceramics, AGH University of Science and Technology, al. Mickiewicza 30, 30-059 Kraków, Poland

Received 23 April 2004; received in revised form 28 June 2004; accepted 6 July 2004
Available online 19 August 2004

Abstract

Various composition of $Na_{1+x}Si_xZr_2P_{3-x}O_{12}$ (x from 1.6 to 2.4), Y-doped Nasicon ($Na_{1+x+y}Zr_{2-y}Y_ySi_xP_{3-x}O_{12}$, $Na_{1+x}Zr_{2-y}Y_ySi_xP_{3-x}O_{12-y}$, where $x = 2$, $y = 0.12$) and Fe-doped Nasicon ($Na_3Zr_{2/3}Fe_{4/3}P_3O_{12}$) were prepared by coprecipitating. Differential thermal analysis (DTA), thermogravimetry (TG), differential scanning calorimetry (DSC), X-ray diffraction (XRD), scanning electron microscopy (SEM) and impedance spectroscopy (IS) were used as experimental techniques.

In order to obtain Nasicon materials free from ZrO_2 admixture, the calcination of coprecipitates must be carried out in proper thermal conditions. The results of DTA, TG and XRD measurements allowed us to propose the best calcination conditions (to obtain mainly Nasicon phases – monoclinic or rhombohedral, depending on composition).

Nasicon-type materials exhibit monoclinic to rhombohedral reversible structural transition, at transition temperature depending on composition (x). The influence of dopants was also studied. The DSC measurements in the temperature range RT–300 °C allowed us to determine the temperatures of this structural transition in the case of $Na_{1+x}Si_xZr_2P_{3-x}O_{12}$, and Y-doped Nasicon. In the case of Fe-doped materials this transition was not detected.

Additionally, the correlation between the composition, microstructure and electrical properties was studied.

Keywords: Nasicon structure; Coprecipitation; Reactivity; DSC; DTA–TG

1. Introduction

Nasicon (Na^+ Super Ionic Conductor) is known to show high ionic conductivity and relatively high chemical stability. This material has been proposed for use as a solid electrolyte in solid-state electrochemical devices such as gas sensors, ion sensors and Na–S batteries [1–3].

Structure of $Na_{1+x}Si_xZr_2P_{3-x}O_{12}$ (x = 0–3) can be described as a three-dimensional network of ZrO_6 octahedra sharing corners with PO_4/SiO_4 tetrahedra. The Na^+ ions are located in the interstitial sites in this framework. Ionic conduction takes place when Na^+ moves from one site to another through "bottlenecks" formed by oxygen ions. Moreover, total electrical conductivity strongly depends on density and nature of the grain boundaries [4–6]. The microstructure of samples is usually affected by the preparation method. Doping can further modify electrical properties of Nasicon materials. For example, the conductivity of yttrium-doped Nasicon is significantly higher that of pure stoichiometric (x = 2) compound [7]. The introduction of Fe^{2+} and Fe^{3+} in the lattice, results in a mixed electronic–ionic conductivity, thus making possible the use as an electrode material [8].

The purpose of this work is to optimize the preparation conditions, and to determine thermal, structural and microstructure properties of Nasicon-type materials with different stoichiometry and dopants (Y, Fe), prepared by coprecipitation and solid-state reaction. Composition, dopants and preparation conditions are believed to influence the structure and microstructure of Nasicon, thus affecting the electrical properties of this material. The preparation of dense, single-phase material with high electrical conductivity is the practical goal of our work.

* Corresponding author. Tel.: +48 12 617 25 26; fax: +48 12 617 24 93.
E-mail address: ignaszak@uci.agh.edu.pl (A. Ignaszak).

0040-6031/$ – see front matter © 2004 Published by Elsevier B.V.
doi:10.1016/j.tca.2004.07.002

2. Materials and methods

$Na_{1+x}Zr_2Si_xP_{3-x}O_{12}$ (x from 1.6 to 2.4), Y-doped ($Na_{1+x+y}Zr_{2-y}Y_ySi_xP_{3-x}O_{12}$, $Na_{1+x}Zr_{2-y}Y_ySi_xP_{3-x}O_{12-y}$, where $x = 2$, $y = 0.12$) and Fe-doped Nasicon ($Na_3Zr_{2/3}Fe_{4/3}P_3O_{12}$) were prepared by coprecipitate method. SiO_2 (POCh, Poland), NaOH (POCh, Poland), $(NH_4)_2HPO_4$ (Aldrich), $ZrO(NO_3)_2$, $Y(NO_3)_3{\cdot}6H_2O$ (Aldrich), $Fe(NO_3)_3{\cdot}9H_2O$ (Aldrich) were used as starting materials.

In addition, Nasicon samples with stoichiometric composition ($x = 2$) were prepared by solid-state reaction of $ZrSiO_4$ (Aldrich) and $Na_3PO_4{\cdot}12H_2O$ (Aldrich). The sample prepared by solid-state reaction was used as reference for the samples prepared by coprecipitation.

Aqueous inorganic salt solutions of $ZrO(NO_3)_2$, NaOH–SiO_2, $(NH_4)_2HPO_4$ for pure, $Y(NO_3)_3$ for yttrium-doped and $ZrO(NO_3)_2$, NaOH, $(NH_4)_2HPO_4$ and $Fe(NO_3)_3$ for Fe-doped NASICON were used for the coprecipitation. All reagents were mixed together and stirred to form a gel-like solid bulk.

The precipitate was then dried for 24 h at temperature slowly increasing to 70 °C and for 12 h at 150 °C. Powders were calcined in two steps: first at 750 °C for 24 h (pure and Y-doped NASICON powders) and 600 °C for 24 h ($Na_3Zr_{2/3}Fe_{4/3}P_3O_{12}$ powders), second at 900 °C for 24 h (pure and Y-doped NASICON pellets) and 700 °C for 24 h ($Na_3Zr_{2/3}Fe_{4/3}P_3O_{12}$ pellets). Powders were ground for about 5 h in 2-propanol using zirconia grinding balls. Then the dried samples were formed into disks with 13 mm diameter and isostatically pressed at 300 MPa. Pure and Y-doped NASICON pellets were finally sintered at $T = 1175$ °C for 5 and 24 h, while $Na_3Zr_{2/3}Fe_{4/3}P_3O_{12}$ pellets were sintered at 800 °C for 3 h.

In the case of solid-state reaction method the mixture of $Na_3PO_4{\cdot}12H_2O$ and $ZrSiO_4$ powders was pressed into pellets before calcination (1150 °C for 24 h). The sample obtained by solid-state reaction was sintered at 1175 °C for 5 h.

Differential thermal analysis (DTA), thermogravimetry (TG) measurements were performed in TA Instruments Derivatograph System, type SDT 2960 in the temperature range 20–1000 °C (heating rates 15 °C/min) under synthetic air atmosphere. Differential scanning calorimetry (DSC) (TA Instruments, model DSC 2010) were performed in the temperature range 20–350 °C (heating or cooling rates 20 °C/min) under synthetic air flow (50 cm^3/min). All experiments were done in alumina 60 mm^3 crucibles.

Scanning electron microscopy (SEM) (JEOL JSM-5400) and X-ray diffraction (XRD) (X'Pert Philips) were used to investigate microstructure and structural properties of prepared samples.

Electrical properties were determined based on ac impedance spectroscopy measurements. Frequency response analyser (FRA) (Solartron, model 1260) coupled with dielectric interface (Solartron, model 1296) were used. Frequency range was 1 Hz–10 MHz, the amplitude of sinusoidal voltage signal was 20 mV. Measurements were done in typical sample holder in synthetic air flow.

Table 1 summarises the composition, preparation conditions and the phase composition of obtained samples.

Table 1
Chemical composition and phase composition of Nasicon samples at different stages of preparation

Sample	$T_{calc.}$ = 750 °C/24 h	$T_{calc.}$ = 900 °C/24 h	$T_{sint.}$ = 1175 °C/24 h
$Na_{2.6}Zr_2Si_{1.6}P_{1.4}0_{12}$ (coprecipitation), $x = 1.6$	ZrO_2 tetragonal	$Na_{2.6}Zr_2Si_{1.6}P_{1.4}0_{12}$ rhombohedral, ZrO_2 tetragonal, ZrO_2 monoclinic (traces)	$Na_{2.6}Zr_2Si_{1.6}P_{1.4}0_{12}$ rhombohedral, ZrO_2 monoclinic
$Na_{2.8}Zr_2Si_{1.8}P_{1.2}0_{12}$ (coprecipitation), $x = 1.8$	ZrO_2 tetragonal	$Na_3Zr_2Si_2P0_{12}$ rhombohedral, ZrO_2 tetragonal, ZrO_2 monoclinic	$Na_{2.88}Zr_{1.68}Si_{1.84}P_{1.16}0_{11.54}$ monoclinic, ZrO_2 monoclinic
$Na_3Zr_2Si_2P0_{12}$ (coprecipitation), $x = 2.0$	ZrO_2 tetragonal	$Na_3Zr_2Si_2P0_{12}$ rhombohedral, ZrO_2 tetragonal, ZrO_2 monoclinic	$Na_3Zr_2Si_2P0_{12}$ monoclinic, ZrO_2 monoclinic
$Na_{3.2}Zr_2Si_{2.2}P_{0.8}0_{12}$ (coprecipitation), $x = 2.2$	ZrO_2 tetragonal	$Na_{3.15}Zr_2Si_{2.15}P_{0.85}0_{12}$ rhombohedral, ZrO_2 tetragonal, ZrO_2 monoclinic, $Na_2ZrSi_2O_7$ (traces)	–
$Na_{3.4}Zr_2Si_{2.4}P_{0.6}O_{12}$ (coprecipitation), $x = 2.4$	ZrO_2 tetragonal	$Na_2ZrSi_2O_7$, ZrO_2 tetragonal, ZrO_2 monoclinic, $Na_{3.35}Zr_2Si_{2.35}P_{0.65}0_{12}$ rhombohedral (traces)	$Na_{3.4}Zr_2Si_{2.4}P_{0.6}O_{12}$ monoclinic, ZrO_2 monoclinic
$Na_3Zr_2Si_2P0_{12}$ (solid-state reaction), $x = 2.0$	–	$T_{calc.}$ = 1150 °C/24 h, $Na_3Zr_2Si_2P0_{12}$, at 25 °C monoclinic, at 300 °C rhombohedral, ZrO_2 monoclinic, $ZrSiO_4$ tetragonal	$Na_3Zr_2Si_2P0_{12}$ monoclinic, ZrO_2 monoclinic, $ZrSiO_4$ tetragonal (traces)
$Na_{3.12}Zr_{1.88}Y_{0.12}Si_2P0_{12}$ (coprecipitation), $x = 2.0$, $y = 0.12$	ZrO_2 tetragonal	$Na_3Zr_2Si_2P0_{12}$ rhombohedral, ZrO_2 tetragonal, ZrO_2 monoclinic	$Na_3Zr_2Si_2P0_{12}$ monoclinic, ZrO_2 monoclinic (traces)
$Na_3Zr_{1.88}Y_{0.12}Si_2P0_{11.88}$ (coprecipitation), $x = 2.0$, $y = 0.12$	ZrO_2 tetragonal	$Na_3Zr_2Si_2P0_{12}$ rhombohedral, ZrO_2 tetragonal, ZrO_2 monoclinic	$Na_3Zr_2Si_2P0_{12}$ monoclinic, ZrO_2 monoclinic (traces)
$Na_3Zr_{2/3}Fe_{4/3}P_30_{12}$ (coprecipitation)	$T_{calc.}$ = 600 °C/24 h, $Na_8Fe_4(PO_4)_6$ not assigned, $NaZr_2(PO_4)_3$ not assigned, $Na_3Fe_2(PO_4)_3$ monoclinic	$T_{calc.}$ = 700 °C/24 h, Fe_2O_3 rhombohedral, $Na_8Fe_4(PO_4)_6$ not assigned, $NaZr_2(PO_4)_3$ not assigned, $Na_3Fe_2(PO_4)_3$ monoclinic	$T_{sint.}$=800 °C/3 h, Fe_2O_3 rhombohedral, $Na_8Fe_4(PO_4)_6$ not assigned, $NaZr_2(PO_4)_3$ not assigned, $Na_3Fe_2(PO_4)_3$ monoclinic

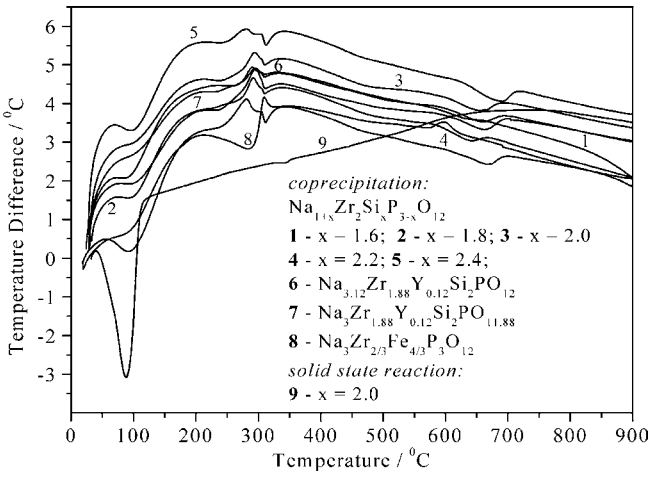

Fig. 1. DTA curves obtained for $Na_{1+x}Zr_2Si_xP_{3-x}O_{12}$ (x = 1.6–2.4), yttrium-doped and iron-doped gel/precipitates (before calcination).

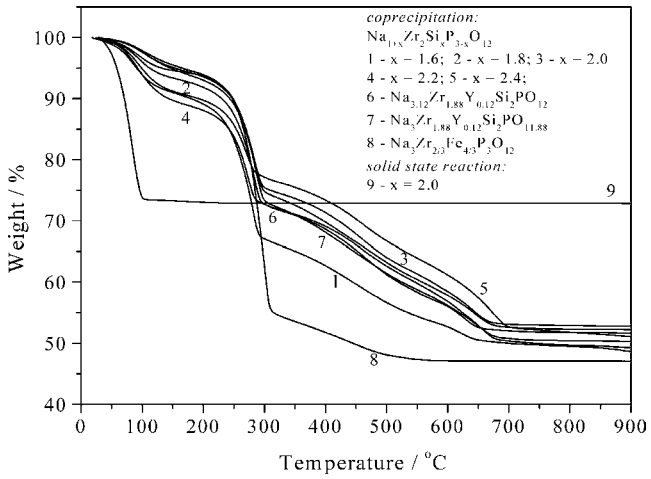

Fig. 2. TG curves obtained for $Na_{1+x}Zr_2Si_xP_{3-x}O_{12}$ (x = 1.6–2.4), yttrium-doped and iron-doped gel/precipitates (before calcination).

The intermediate products and final samples (after calcination/sintering) were used for further characterization.

3. Results and discussion

3.1. Influence of preparation conditions

Figs. 1 and 2 show the DTA and TG curves obtained for Nasicon samples with different stoichiometry (x), dopants (Y, Fe) or prepared using different methods (coprecipitation, solid-state reaction). Fig. 3 shows the comparison of X-ray diffraction data obtained for Nasicon samples with $x = 2$, after calcination at different temperatures.

As can be seen in Fig. 1, the DTA curves obtained for samples with different stoichiometry (x) and yttrium-doped samples exhibit similar behaviour. According to literature data [18], the group of endo- and exo-thermal peaks in the range from 275 to 325 °C corresponds to decomposition of NH_4NO_3 formed as a by-product during the preparation procedure. The broad endo-thermal peak in the temperature range 650–720 °C may be attributed to the formation of ZrO_2 phase, which is an intermediate product of Nasicon-phase formation. According to XRD data presented in Fig. 3, the calcination of primary gel/coprecipitate at the temperature T = 750 °C leads to the formation of nanocrystalline tetragonal ZrO_2, and no traces of other phases are observed. Further calcination at T = 900 °C followed by T = 1175 °C leads to the formation of Nasicon phases (tetragonal) with slight admixture of monoclinic ZrO_2 phase. The thermal effect of formation of Nasicon phases at higher temperatures was not observed on DTA curves.

The temperature ranges of observed DTA peaks correspond well to the changes of TG curves, as shown in Fig. 1.

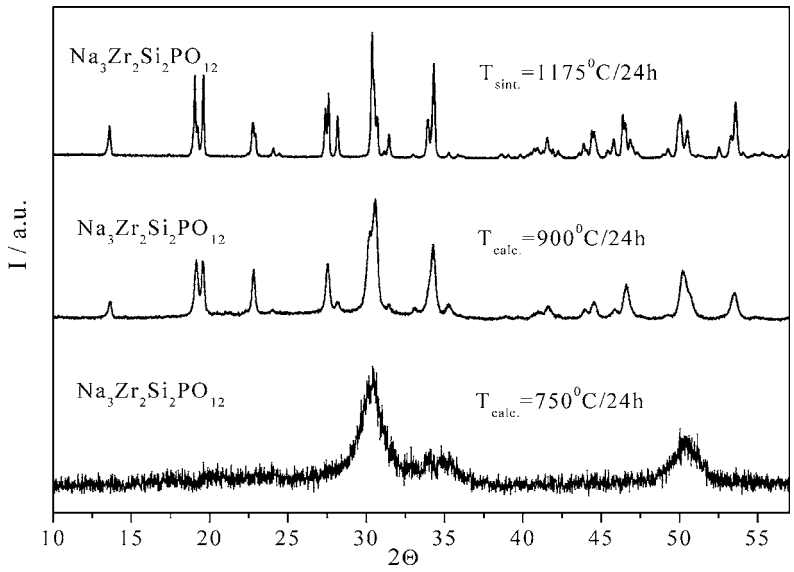

Fig. 3. XRD patterns of $Na_3Zr_2Si_2PO_{12}$ sample prepared by coprecipitation, as a function of calcination/sintering temperature.

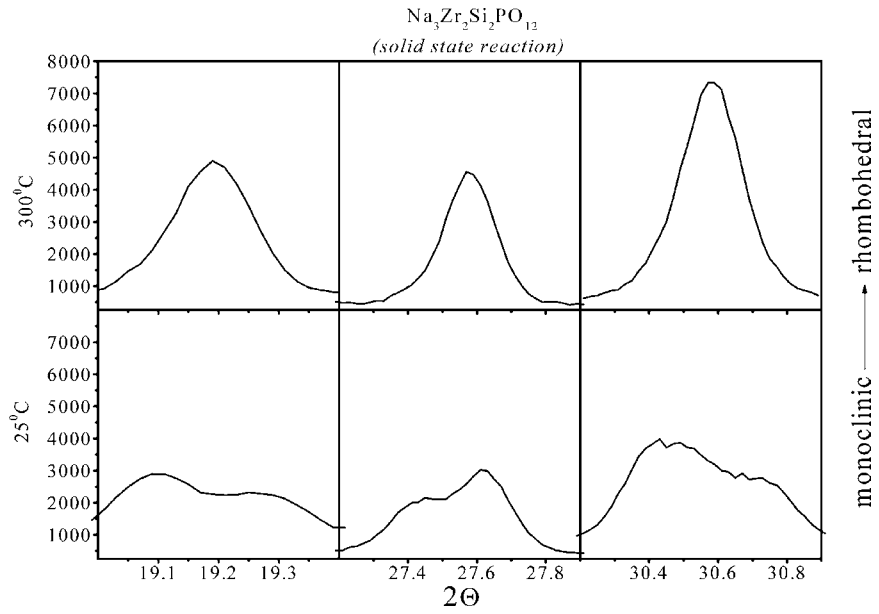

Fig. 4. Phase transition shown on detailed XRD patterns of $Na_3Zr_2Si_2PO_{12}$ sample prepared by solid-state reaction, measured at 25 and 300 °C.

The most intensive weight loss can be observed in the range of T = 275–325 °C (NH_4NO_3 removal), and finishes at about T = 700 °C.

In the case of Fe-doped sample the observed DTA and TG behaviour is similar to that described above, suggesting related mechanism of Nasicon-type structure formation in this case. Some apparent differences caused by clearly different chemical composition can be noticed, but detailed discussion is not possible without additional investigations.

During the preparation of Nasicon sample (with x = 2) by solid-state reaction method only one DTA peak at about T = 100 °C can be observed, as shown in Fig. 1. It is accompanied by the weight loss, as can be seen in Fig. 2, and can be interpreted in terms of dehydration of $Na_3PO_4{\cdot}12H_2O$ used as one of starting materials.

Nasicon-type materials may exhibit monoclinic to rhombohedral reversible structural transition. This structural transition can be observed by the modification of XRD spectra with temperature, as shown in Fig. 4 (Nasicon sample, x = 2, solid-state reaction, calcination at T = 1150 °C). As can be seen, the reflex observed for the high-temperature rhombohedral phase (measurement at T = 300 °C) split into two reflexes of low-temperature monoclinic phase (measurement at T = 25 °C). This splitting was not observed for powders calcined at 900 °C (coprecipitation method).

The described transition is accompanied by a thermal effect and can also be observed on DSC curve. For $Na_3Zr_2Si_2P_{3-x}O_{12}$ (x = 2) samples prepared by both coprecipitate and solid-state reaction methods (sintering at 1150 °C for 24 h) the structural transition temperature is the same (T = 165 °C) and does not depend on preparation method.

3.2. Influence of stoichiometry (x)

In order to discuss the influence of stoichiometry (x) the XRD and DSC measurements were performed on samples with different compositions. Fig. 5 shows the XRD data obtained for these samples, prepared by coprecipitation method, calcined at T = 900 °C and sintered at T = 1175 °C. XRD data concerning the sample prepared by solid-state reaction (x = 2, sintered at T = 1175 °C) are also included as a reference.

In the case of samples prepared by coprecipitate method and sintered at T = 1175 °C the obtained XRD spectra show the complete crystallisation of Nasicon phases, as shown in Fig. 5 (while the samples after the calcination are not well crystallised). The sample with composition x = 1.6 crystallises in rhombohedral structure, while the other Nasicon samples (x = 2.4, 2.2, 2.0 and 1.8) crystallise in monoclinic structure. There is almost no difference in XRD spectra obtained for these two types of structures, so they are hardly observable in Fig. 5. The difference may be only observed as splitting of selected reflexes, as shown in Fig. 4. The XRD spectra obtained for Nasicon sample prepared by solid-state reaction method (x = 2) also indicate the monoclinic phase, with traces of tetragonal $ZrSiO_4$ phase and slight admixture of monoclinic ZrO_2 phase. The presence of monoclinic ZrO_2 was also detected in samples prepared by coprecipitate method.

The results concerning the phase composition of Nasicon samples with different composition, and prepared at different conditions will be summarised in Table 1, in the next part of this paper.

Fig. 6 shows the DSC curves obtained for Nasicon samples with different stoichiometry, x, prepared by coprecipitation method and sintered at T = 1150 °C. Mono-

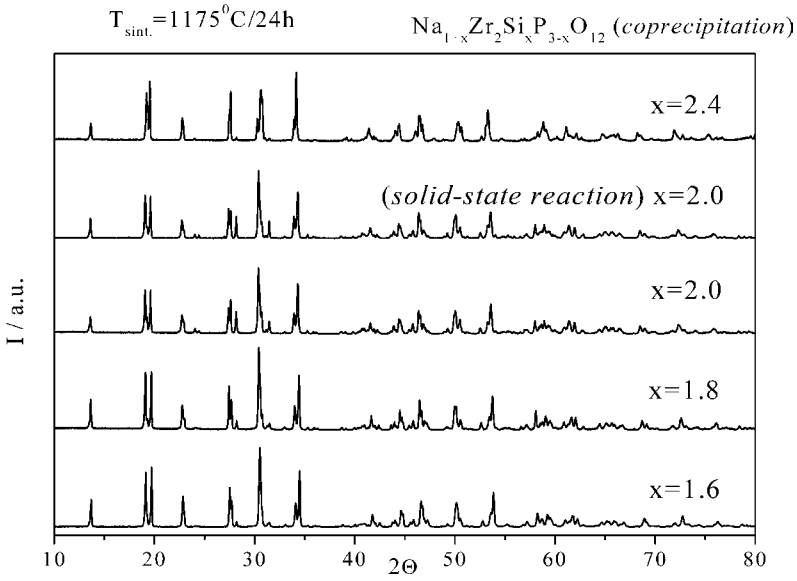

Fig. 5. XRD patterns of $Na_{1+x}Zr_2Si_xP_{3-x}O_{12}$ (x = 1.6–2.4) pellets sintered at 1175 °C/24 h (coprecipitation, solid-state reaction).

clinic to rhombohedral structural transition is observed for $Na_{1+x}Zr_2Si_xP_{3-x}O_{12}$ (x from 1.8 to 2.4), but in the case of sample with x = 1.6 this effect does not appear. As can be seen, the transition temperature depends on the composition of samples (x), reaching the highest value for sample with x = 2.

3.3. Influence of Y and Fe dopants

In the case of Y-doped Nasicon powders after calcination at 900 °C no differences in XRD data can be detected in comparison to undoped material. The rhombohedral Nasicon structure was found as main phase. Substituting with iron leads to modification of the structure, which can be considered as mixture of solid solutions of $Na_8Fe_4(PO_4)_6$, $NaZr_2(PO_4)_3$ and $Na_3Fe(III)_2(PO_4)_3$ Nasicon-like phases [9]. Also, some rhombohedral Fe_2O_3 is present.

The following sintering at T = 1175 °C of doped Nasicon materials leads to further crystallisation of materials. In the case of yttrium-doped samples the monoclinic Nasicon phase is observed, as in the case of undoped Nasicon (x = 2). Also, the presence of monoclinic ZrO_2 can be detected, but the addition of yttrium dopant seems to decrease the intensity of its reflexes. In the case of Fe-doped sample no modification of XRD spectra can be noticed, comparing to the spectra obtained for the sample calcined at T = 700 °C.

Fig. 7 shows the comparison of DSC curves recorded for the yttrium-doped and iron substituted Nasicon samples with the undoped sample with stoichiometric composition (x = 2), sintered at T = 1150 °C (in the case of Y-doping) and at T = 800 °C (in the case of Fe-doping).

As can be noticed, in the case of yttrium-doped Nasicon pellets the transition temperature decreases comparing to the

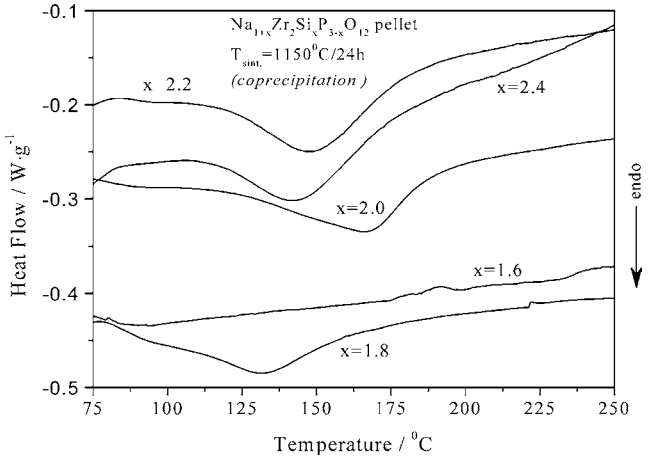

Fig. 6. DSC curves for $Na_{1+x}Zr_2Si_xP_{3-x}O_{12}$ samples with different composition (x = 1.6–2.4) (scan rate 20 °C/min, measurement in flow of synthetic air).

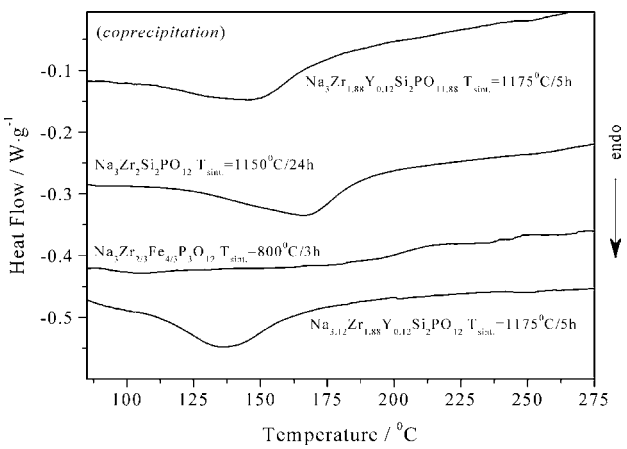

Fig. 7. DSC curves of undoped, Y-doped and Fe-doped Nasicon pellets (scan rate 20 °C/min, measurement in flow of synthetic air).

stoichiometric (x = 2) electrolyte, while in the case of Fe-doped Nasicon this structural transition is not observed. The explanation of these results should comply with the hypothesis [10] that the monoclinic to rhombohedral transition can be related to the local lattice distortion caused by Zr^{4+} ions displacement from its proper sites and formation of additional Na^{+} interstitial positions (mid-Na [10,11]) between two Zr^{4+} sites. In case of undoped Nasicon the monoclinic to rhombohedral transition takes place only in limited range of stoichiometry, x ($1.8 \leq x \leq 2.4$ [12] or $1.6 < x < 2.2$ [13]). The replacement of some Zr atoms by Y or Fe may partially or even completely prevent such distortion thus leading to the change of transition temperature or even disappearance of such transition.

3.4. Microstructure and electrical properties

Fig. 8 shows the comparison of SEM microphotographs taken for samples with different composition (dopants) or prepared by different methods. The comparison of images A and B indicate that sample prepared by solid-state reaction exhibits higher density. In case of samples prepared by copre-

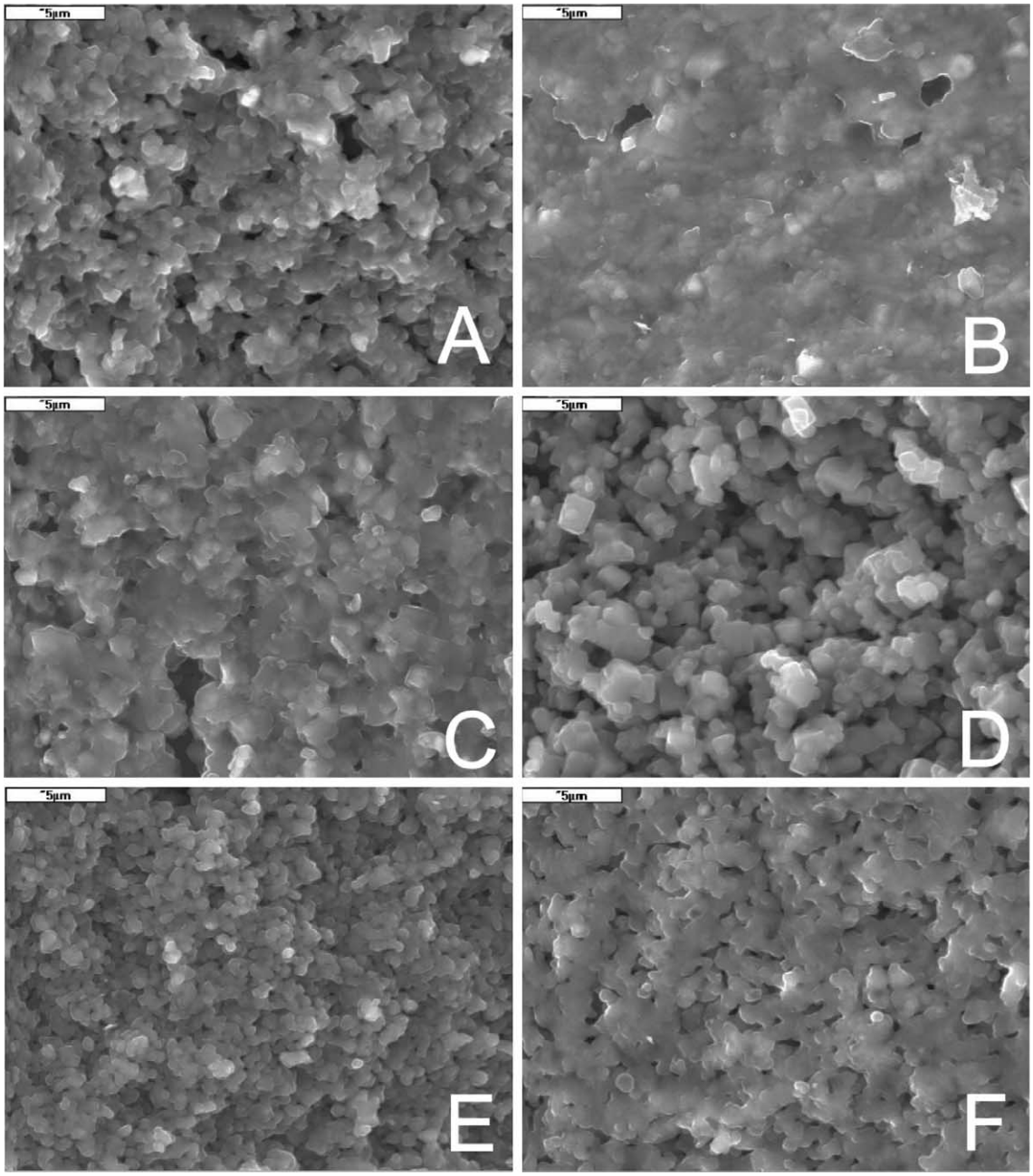

Fig. 8. SEM micrographs of $Na_3Zr_2Si_2PO_{12}$ pellets sintered at 1175 °C/5 h (A: coprecipitation, B: solid-state reaction), C: $Na_{2.6}Zr_2Si_{1.6}P_{1.4}O_{12}$, D: $Na_{3.4}Zr_2Si_{2.4}P_{0.6}O_{12}$ pellets sintered at 1175 °C/5 h (coprecipitation), E: $Na_3Zr_{2/3}Fe_{4/3}P_3O_{12}$ pellet sintered at 800 °C/3 h (coprecipitation), F: $Na_3Zr_{1.88}Y_{0.12}Si_2P0_{11.88}$ pellet sintered at 1175 °C/5 h (coprecipitation).

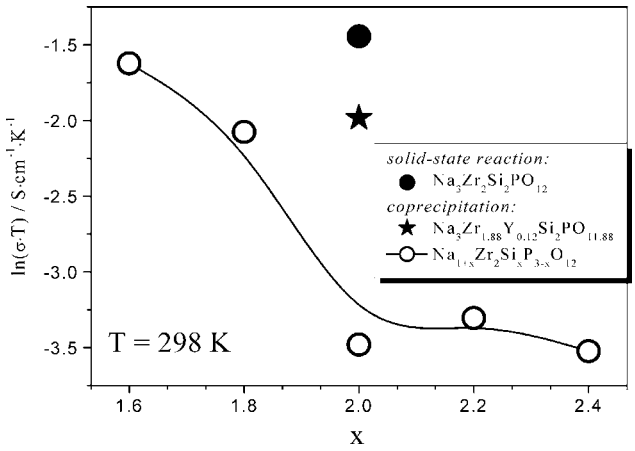

Fig. 9. Electrical conductivity as a function of temperature of Nasicon samples, measured at $T = 298$ K, in synthetic air flow.

cipitation the introduction of yttria leads to remarkable improvement of the sample (Fig. 8A and F). The microstructure depends on composition, x (Fig. 8A, C and D). The introduction of Fe into Nasicon leads to completely different microstructure of samples. Fe-doped sintered material is highly porous and consists of fine grains (Fig. 8E).

Fig. 9 shows the dependence of total electrical conductivity of the same samples as shown in Fig. 8, measured at room temperature. As can be seen the total electrical conductivity depends on composition, x, and can be correlated with the microstructure of obtained samples (see Fig. 8). The highest electrical conductivity was observed for Nasicon prepared by solid-state reaction method and Y-doped material. Both samples exhibit higher density comparing to the undoped sample prepared by coprecipitation method with $x = 2$.

The presented results indicate clearly that the higher density of obtained material, the higher electrical conductivity measured at room temperature. Most authors [13–15] observe the highest electrical conductivity in the case of samples with $x = 2$–2.2, which is in apparent disagreement with our results. It can be explained by different contribution of grain boundaries and bulk conductivities to the total electrical conductivity in different temperature ranges. At lower temperatures (as in our case) the properties of grain boundaries are predominating and the density of samples is the most important factor controlling the total electrical conductivity. At higher temperatures [6,16,17] the bulk conductivity, which is dependent on the composition, is responsible for the total electrical conductivity.

In order to avoid misunderstanding the results concerning electrical conductivity of Fe-doped Nasicon were not shown in Fig. 9 in comparison with other samples. This material is expected to be mixed ionic–electronic conductor (also different type of mobile ions are possible) [9], contrary to the purely ionic Nasicon conductors and thus the absolute vales of total electrical conductivities cannot be compared directly. More detailed studies are under the way, the results will be published later.

4. Conclusions

The results obtained from DTA, TG and XRD measurements allowed to discuss the reactions taking place during the preparation procedure and thermal and structural properties of obtained products at every stage of preparation.

The DSC measurements in the temperature range RT–300 °C allowed us to determine the temperatures of this structural transition only for the material sintered at 1150 °C (case of $Na_{1+x}Si_xZr_2P_{3-x}O_{12}$), and Y-doped Nasicon. In the case of Fe-doped material this transition was not observed.

In order to obtain Nasicon materials free from ZrO_2 phase admixture, the calcination of coprecipitates must be done in proper thermal conditions. The obtained results allowed us to optimize the calcination conditions (1175 °C for 5 h), where almost pure Nasicon phase (monoclinic or rhombohedral, depending on composition) is obtained.

The results of SEM observations and electrical conductivity measurements allowed us to determine the correlation between the microstructure and the electrical properties of the samples investigated. Namely, the higher density of obtained material, the higher electrical conductivity (measured at room temperature). These results indicate in general that different correlations between composition, dopants and preparation conditions must be taken into account during optimization of material properties.

The case of Nasicon samples doped with Fe is more complex and needs further studies in order to determine the proper preparation conditions leading to its potential application as an electrode material.

Acknowledgements

The financial support of Polish State Committee for Scientific Research (KBN), Project No. 7 T08A 03021 is acknowledged.

References

[1] D.D. Lee, S.D. Choi, K.W. Lee, Sens. Actuators B 24/25 (1995) 607–609.
[2] T. Kida, Y. Miyachi, K. Shimanoe, N. Yamazoe, Sens. Actuators B 80 (2001) 28–32.
[3] E. Traversa, H. Aono, Y. Sadaoka, L. Montanaro, Sens. Actuators B 65 (2000) 204–208.
[4] U. von Alpen, Mater. Res. Bull. 14 (1979) 1317–1322.
[5] H. Perthuis, P. Colomban, Ceram. Int. 12 (1986) 39–52.
[6] O. Bohnke, S. Ronchetti, D. Mazza, Solid State Ionics 122 (1999) 127–136.
[7] O. Nakamura, Y. Saito, M. Kodama, Y. Yamamoto, Solid State Ionics 89 (1996) 159–164.
[8] R.O. Fuentes, F.M. Figueiredo, F.M.B. Marques, J.I. Franco, J. Eur. Ceram. Soc. 21 (2001) 737–743.
[9] O. Tillement, J. Angenault, J.C. Couturier, M. Quarton, Solid State Ionics 44 (1991) 299–303.
[10] J.P. Boilot, Ph. Colomban, G. Collin, Solid State Ionics 28–30 (1988) 403–410.

[11] G. Collin, R. Come, J.P. Boilot, P. Colomban, Solid State Ionics 28–30 (1988) 427–431.
[12] U. von Alpen, M.F. Bell, H.H. Hőfer, Solid State Ionics 3/4 (1981) 215–218.
[13] J.P. Boilot, J.P. Salanié, G. Desplanches, D. Le Potier, Mater. Res. Bull. 14 (1979) 1469–1477.
[14] D. Tran Qui, J.J. Capponi, M. Gondrand, M. Saïb, J.C. Joubert, R.D. Shannon, Solid State Ionics 3/4 (1981) 219–222.
[15] J.P. Boilot, G. Collin, Ph. Colomban, J. Solid State Chem. 73 (1988) 160–171.
[16] W. Bogusz, F. Krok, W. Jakubowski, Solid State Ionics 2 (1981) 171–174.
[17] W. Bogusz, F. Krok, W. Piszczatowski, Solid State Ionics 119 (1999) 165–171.
[18] Y. Schimizu, T. Ushijima, Solid State Ionics 132 (2000) 143–148.